Electrically Small Antenna with Embedded Operational Amplifier Circuit Surpasses the Passive Upper Bound of the Gain-Bandwidth Product

Yaqing Yu [1], Ming-Chun Tang [1], Da Yi [1], Dingmou Hong [1], Ting Shi [1], and Richard W. Ziolkowski [2]
[1] Chongqing University, College of Microelectronics and Communication Engineering, Chongqing, China,
tangmingchun@cqu.edu.cn
[2] University of Technology Sydney, Global Big Data Technologies Centre, Ultimo NSW, Australia,
Richard.Ziolkowski@uts.edu.au

***Abstract*—A near-field resonant parasitic (NFRP) active electrically small transmitting antenna is reported in this paper. It consists of an electrically small NFRP antenna and an operational amplifier (OpAmp). In the design, the NFRP element serves as the main radiator and the feedback pathway of the OpAmp simultaneously, i.e., the electrically small antenna (ESA) and the OpAmp circuit are arranged within a shared ultra-compact space. This configuration significantly increases the effective gain of the ESA without consuming any additional real estate. The overall electrical size of its radiating element is extremely small with $ka = 0.15$ at 414 MHz, i.e., $a \approx \lambda/42$. The measured results of this active ESA, in good agreement with their simulated values, demonstrate that its effective gain can be dynamically tuned within a 6.01 dB range. Compared with its corresponding passive counterpart, the measured maximum effective gain and hence, the effective isotropic radiated power (*EIRP*) of our developed active ESA witnesses a 9.152 dB (8.23 times) improvement. Thus, the measured gain-bandwidth product (*GBWP*) surpasses the corresponding passive Bode-Fano upper bound by approximately 15.2 times.**

***Index Terms*—Electrically small antennas (ESAs), gain, near-field resonant parasitic (NFRP) elements, operational amplifier (OpAmp).**

I. INTRODUCTION

Electrically small antennas (ESAs) have always been a hot research topic because their sizes are electrically small in comparison to their corresponding operational wavelengths. This feature makes them suitable for a wide variety of wireless applications [1]-[4]. However, the basic physics associated with their electrically small sizes inherently limits their performance characteristics, e.g., their impedance bandwidths and realized gain values. Those bounds are described by Bode-Fano theory [5], [6] and the Chu-Wheeler-Harrington limits [7]-[9]. As a consequence, active non-Foster circuits [10], [11] have been considered to significantly extend the operating bandwidth of an ESA while maintaining its radiation performance.

In order to improve the realized gain values of ESAs, many approaches, such as Yagi-configurations [12], introducing superstrates [13], near-field resonant parasitic (NFRP) elements [14], [15] and Huygens dipole antennas [16]-[18] have been investigated. While effective, the improvement of their gain values still witnesses certain limitations when the antenna volumes are quite constrained, e.g., when $ka < 0.2$ (a is the radius of the smallest sphere enclosing the entire radiator system and k is the free-space wavenumber at the resonant frequency f_0). The maximum gain value of such an ESA is generally quite low, e.g., –15 dBi [19]. Consequently, such low realized gain values make it difficult to justify their application in many space-constrained high-gain transmission platforms, particularly where large signal attenuation is involved and high-gain transmission becomes necessary. Practical scenarios include the Internet of Things (IoT) [20] and smart home wireless access [21] in which wireless devices must operate in the presence of thick reinforced concrete walls, varying atmospheric conditions and high multipath noise levels.

On the other hand, it has been demonstrated that active circuits can be utilized to achieve a significant increase of the effective bandwidth and gain of a passive wireless system. A common method employs a single active amplifier circuit module that is directly cascaded with a passive antenna to achieve those enhancements [22]-[25]. However, this cascade approach significantly increases the system's overall size. Consequently, it is not generally suitable to achieve an overall electrically small design.

In this paper, an innovative approach is described that seamlessly integrates an active circuit with a passive radiator to enhance its effective gain. The system is developed by co-designing a NFRP ESA naturally augmented with an operational amplifier (OpAmp) circuit. The NFRP element is introduced into the OpAmp circuit in a manner that does not increase the overall occupied space. The NFRP element has two functions. On one hand, it functions as the main radiator of the ESA system [14, 15]. On the other hand, it serves as a lossy resonator in the feedback loop which facilitates the tunability of the effective gain of the entire ESA system. Importantly, the consequent active ESA maintains the ka value of the passive counterpart, attains a maximum effective gain of 7.232 dBi, and a gain-bandwidth product (*GBWP*) of 0.0513, which surpasses the corresponding passive Bode-Fano upper bound by 15.2 times. Hence, it would be a good candidate for many space-constrained wireless scenarios.

II. Design of the Effective Gain Enhanced ESA

A. Basic Design Principle

The general configuration of an ideal non-inverting OpAmp circuit and a NFRP ESA is illustrated in Figs. 1(a) and 1(b). In a conventional front-end system, the amplifiers and the ESAs are individually designed and then cascaded. This technique inevitably leads to an increase of the occupied area/volume. To address this size issue, we have found that the two individual components can be combined effectively in a shared space as depicted in Fig. 1(c). Clearly, the NFRP ESA is embedded in the feedback loop of the OpAmp circuit.

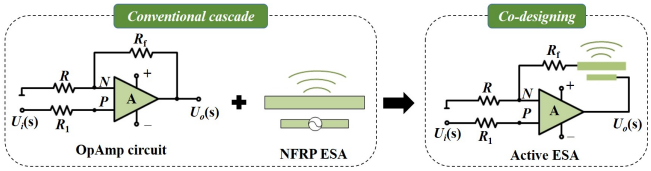

Fig. 1. Configurations of active NFRP ESAs. (a) OpAmp circuit. (b) NFRP antenna in series with the OpAmp. (c) NFRP antenna embedded in the negative feedback loop of the OpAmp circuit.

B. Active ESA configulation and Performance Analysis

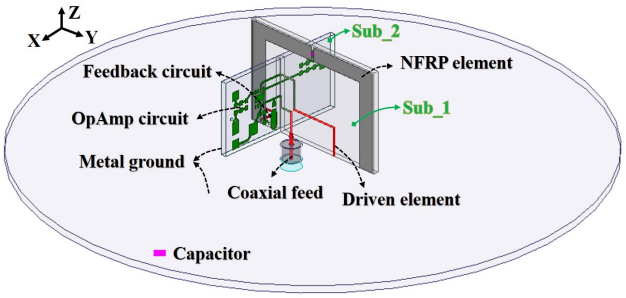

Fig. 2. The proposed active ESA configuration

The realization of this unconventional arrangement in which the two individual components are combined in a co-shared volume is presented in Fig. 2. The system consists of an active OpAmp circuit and a modified version of the 2D magnetic EZ ESA introduced in [26] in which the NFRP element is a capacitively loaded loop (CLL) and the driven element is a coax-fed semi-loop antenna. The NFRP element and the driven element are printed on a rectangular piece of Rogers Duroid™ 5880, labeled as Sub_1, which has a thickness h_1 = 0.787 mm. The NFRP element is excited by the driven element and is the primary radiator. One end of the driven element and both ends of the NFRP element are connected to the ground plane. The OpAmp circuit is printed on Sub_2, which is another rectangular piece of the Rogers 5880 substrate with the same permittivity and thickness as Sub_1. Note that the driven semi-loop element is split at the first right angle of the trace from the coax to create a small gap. The consequent two pieces of the semi-loop are then connected to the positive input and output ports of the OpAmp. The NFRP element thus becomes as a major part of the feedback loop of the OpAmp circuit.

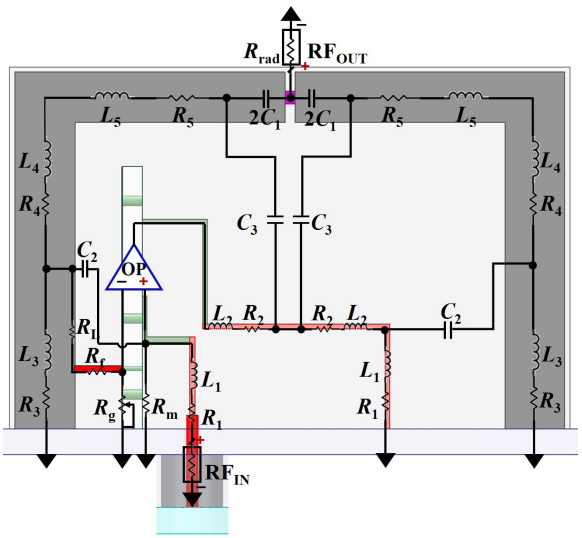

Fig. 3. Effective circuit based on the physical structure of the active ESA.

The operating mechanisms of the active ESA are revealed by building the corresponding effective circuit model based on its physical structure. This model is presented in Fig. 3. Specifically, the semi-rectangular loop driven element is modeled by as a series circuit consisting of four lossy inductors together with four resistors. Similarly, the semi-rectangular loop NFRP element is equivalent to a symmetric series circuit that includes six inductors and six resistors loaded with one capacitor. The radiation resistance of the ESA is represented by the grounded resistor. The capacitive coupling between the driven element and NFRP element is represented by four capacitors. The various components of the OpAmp circuit are connected to NFRP element. It is important to emphasize that the so-called "effective gain" (see [27], [28]) will be utilized herein to evaluate the gain performance of the active ESA. On the other hand, the "realized gain" will be used for its passive counterpart. Moreover, the effective gain of the system is proportional to the radiated power, i.e., the power associated with the radiation resistance. Therefore, we set the radiation resistance as another port and check the simulated $|S_{21}|$ values of the circuit to clearly observe the effective gain enhancement performance of the active ESA.

The simulated $|S_{21}|$ values for different R_g values are plotted in Fig. 4. According to these simulation results, one can see that the $|S_{21}|$ values of the effective circuit can be dynamically tuned within a Δ = 6.3 dB range by regulating the adjustable resistor R_g value from 5 Ω to 2000 Ω. In

particular, the peak $|S_{21}|$ value of the effective circuit model is 7.49, 6.01, 4.53, 3.17, 2.02, and 1.18 dB when the R_g is 5, 200, 400, 700, 1200 and 2000 Ω, respectively.

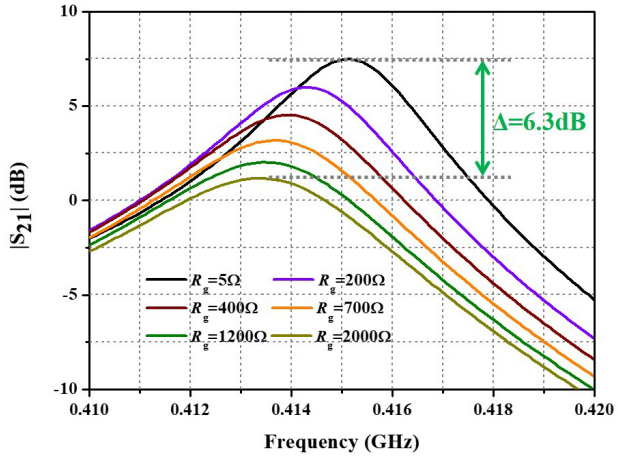

Fig. 4. Simulated $|S_{21}|$ of the effective circuit with different values of the resistor R_g.

III. Measurement of the Proposed Active ESA

The optimized active ESA shown in Fig. 2 was fabricated, assembled, and measured. The fabricated prototypes are shown in Figs. 5(a) and 5(b). The antenna under test (AUT) in the measurement chamber is shown in Fig. 5(c).

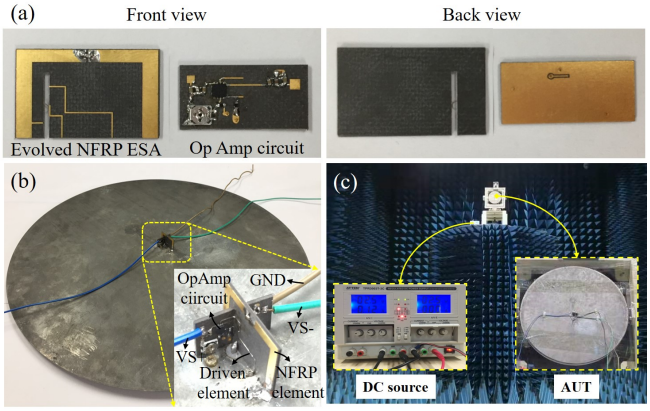

Fig. 5. Fabricated active ESA. (a) Front and back views of each layer before assembly, (b) 3-D isometric view, (c) Antenna under test (AUT) in the chamber.

The measured S-parameters and gain responses of the active ESA prototype are presented in Fig. 6. These results are given at six different R_g values of the adjustable resistor, i.e., R_g = 5 Ω, 200 Ω, 400 Ω, 700 Ω and 2000 Ω. One finds that the $|S_{11}|$ curves of the active ESA are below –10 dB over the whole band. This behavior results from the 50 Ω resistance present at the positive input port of the OpAmp for impedance matching. Notice that these curves reach their minimum values near the same working frequency, i.e., near 414 MHz. This outcome indicates that the frequency offsets of the six different cases can be ignored. The measured effective gain curves of the active ESA also demonstrate a variation similar to the corresponding effective circuit model results shown in Fig. 4. These results further verify the effectiveness of our developed design principle. We also note that the 3-dB bandwidths of the measured effective gain curves are greatly enlarged. This complementary result occurs because of the frequency-dependent amplification of the OpAmp circuit, i.e., the larger amplification can compensate for the smaller realized gain in the neighborhood of the working frequency of the passive ESA, thus expanding the bandwidth [29].

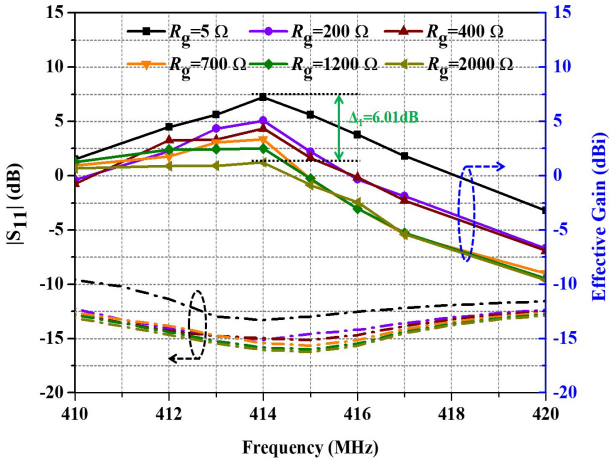

Fig. 6. The measured $|S_{11}|$ (dashed lines) and effective gain values (solid marked lines) of the active ESA at different resistor R_g values.

The peak effective gain for different R_g values was extracted from the measured results to clearly demonstrate how the R_g value regulates the effective gain. These results are shown in Fig. 7 (the violet line). The measured peak effective gain values of the active ESA are 7.232 dBi, 5.07 dBi, 4.352 dBi, 3.339 dBi, 2.498 dBi, and 1.222 dBi, when R_g = 5 Ω, 200 Ω, 400 Ω, 700 Ω, 1200 Ω and 2000 Ω, respectively, at the center frequency 414 MHz. The measured fractional bandwidth (*FBW*) associated with the –3 dB points of the active ESA equals 0.966% [30], [31]. These results clearly illustrate the dynamic adjustability of the effective gain of the active ESA. Hence, the maximum effective isotropic radiated power (*EIRP*), which is defined as the product of P_{in} and G_{ant} (where P_{in} and G_{ant} are the input power delivered to the antenna and the gain of the antenna, respectively) of the developed active transmitting ESA witnessed an 8.23 times improvement in comparison to its passive counterpart [32]. Therefore, the Δ_1 = 6.01 dB variation of the effective gain and the improved *EIRP* demonstrate that the developed *ka* = 0.15 active ESA can meet the requirements of a variety of high-gain, narrow-

band transmission applications in space-constrained wireless platforms.

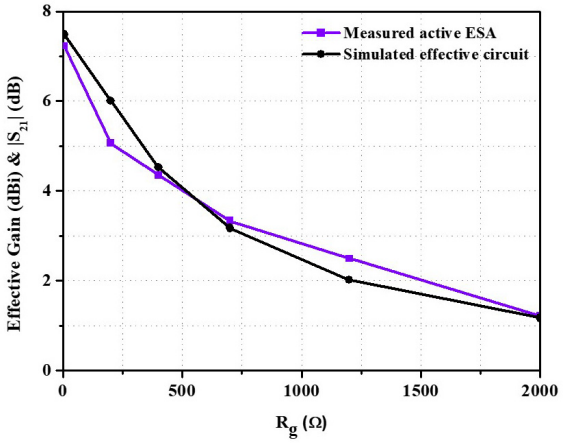

Fig. 7. The measured effective gain values of the active ESA at six different resistor R_g values (violet line) and the simulated $S|_{21}|$ of the effective circuit at different resistor R_g values (black line).

The *GBWP* of the ESA prototype can be derived from [30], [31], [33], [34], i.e., it is the product: $GBWP_{\text{measured.}} = G_{\max} \times FBW_{3\text{dB}}$. The peak effective gain of the active ESA is 7.232 dBi = 5.287 which occurs when R_g = 5 Ω. The corresponding $FBW_{3\text{dB}}$ = 0.00966. This means $GBWP_{\max, \text{measured}}$ = 5.287 × 0.00966 = 0.0513. The passive ESA has the maximum upper bound on its $(GBWP)_{\max, \text{passive}} = D_{\max} \times FBW_{3\text{dB}} \leq (ka)^3 = (0.15)^3 = 3.375\times10^{-3}$ [33]-[36]. Thus, the measured active ESA had a 15.2 times enhancement of the $GBWP_{\max}$ value in comparison to its passive counterpart.

The co-polarization and cross-polarization radiation patterns of the active ESA in the *E*-plane (*yoz*) and *H*-plane (*xoz*) measured at its operational frequency 414 MHz under different R_g values are exhibited in Fig. 8. The peak effective gain values are located at the azimuth = 0°. The measured cross-polarization levels are 15 dB lower than the co-polarization levels, demonstrating that a high polarization purity was obtained. It is worth noting that uniform and stable gain patterns were obtained in all of these cases. This feature further demonstrates that the OpAmp circuit has little influence on the shape of the patterns even though it has a large impact on their peak values.

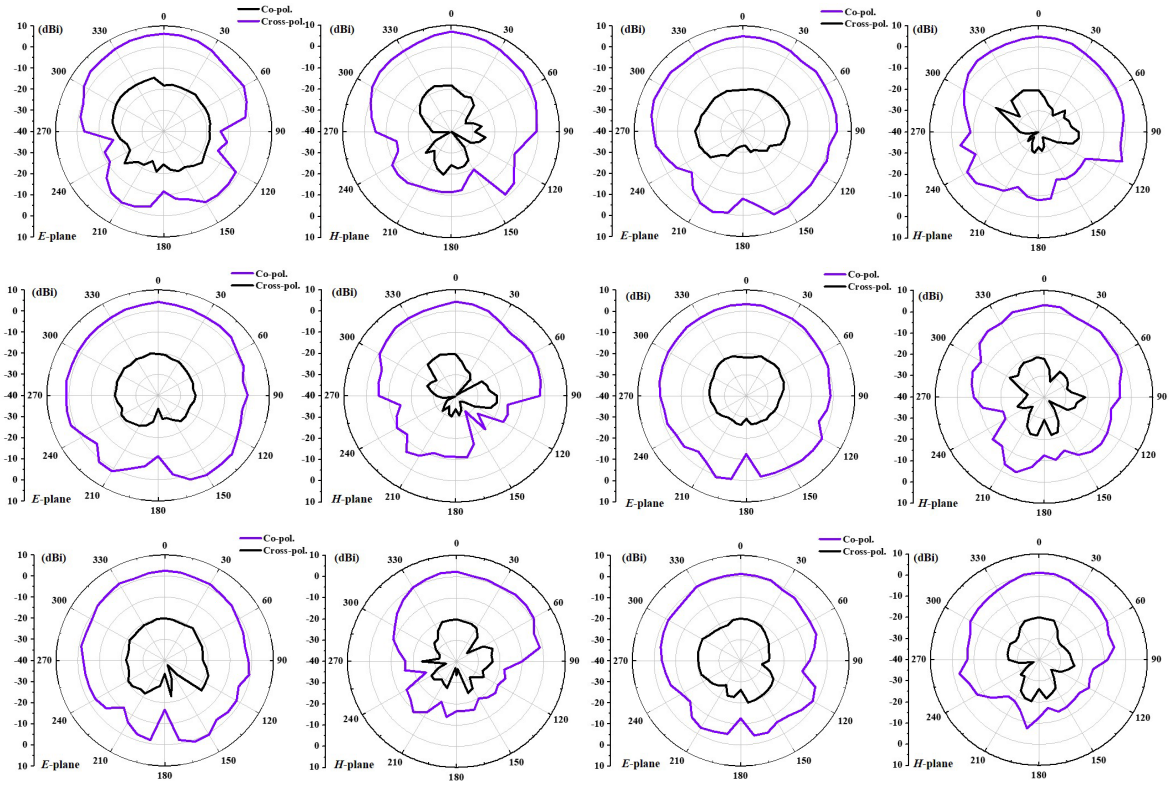

Fig. 8. The measured effective gain patterns of the prototype active ESA operating at 414 MHz with six different resistor values R_g; (a) R_g = 5 Ω, (b) R_g = 200 Ω, (c) R_g = 400 Ω, (d) R_g = 700 Ω, (e) R_g = 1200 Ω, (f) R_g = 2000 Ω.

IV. Conclusions

An effective-gain-enhanced electrically small NFRP antenna with *ka* = 0.15 was designed and its simulated performance characteristics were experimentally verified. With an innovative seamless integration approach, i.e., by embedding the NFRP element of this active ESA in the negative feedback loop of an OpAmp circuit, its effective gain was significantly improved in comparison to its passive counterpart while the overall electrically small size was

maintained. The measured results, in good agreement with the simulated values of the effective circuit, validated its efficacy. Furthermore, the capability to adjust the system's effective gain from 1.222 to 7.232 dBi was attained by simply adjusting the value of the resistor R_g from 5 to 2000 Ω in the feedback loop. Thus, the maximum *EIRP* of the active ESA was 8.23 times larger than that of its passive counterpart. More importantly, the active ESA produced an experimentally validated maximum *GBWP* that is 15.2 times larger than the upper bound of its passive counterpart. Benefitting from these attractive performance characteristics, the developed active ESA is a potentially viable solution for future space-constrained narrow-band wireless applications requiring a high effective gain.

REFERENCES

[1] R. W. Ziolkowski, and A. Erentok, "Metamaterial-based efficient electrically small antennas," IEEE Trans. Antennas Propag., vol. 54, no. 7, pp. 2113–2130, Jul. 2006.

[2] R. W. Ziolkowski, "An efficient, electrically small antenna designed for VHF and UHF applications," IEEE Antennas Wireless Propag. Lett., vol. 7, pp. 217–220, 2008.

[3] M. -C. Tang, B. Y. Zhou, and R. W. Ziolkowski, "Flexible uniplanar electrically small directive antenna empowered by a modified CPW-feed," IEEE Antennas Wireless Propag. Lett., vol. 15, pp. 914–917, 2016.

[4] S. Lim, J. X. Chen, and C. Cato, "Design of a thin, electrically small, two-element parasitic array with circular polarization," IEEE Antennas Wireless Propag. Lett., vol. 17, pp. 1006–1009, 2018.

[5] H. Bode, Network Analysis and Feedback Amplifier Design. New York: Van Nostrand, 1947.

[6] R. M. Fano, "Theoretical limitations on the broadband matching of arbitrary impedances," J. Franklin Inst., vol. 249, pp. 139–154, Feb.1950.

[7] L. J. Chu, "Physical limitations of omni-directional antennas," J. Appl. Phys., vol. 19, no. 12, pp. 1163–1175, 1948.

[8] H. A. Wheeler, "Fundamental limitations of small antennas," Proc. IRE, vol. 35, no. 12, pp. 1479–1484, Dec. 1947.

[9] R. F. Harrington, "Effect of antenna size on gain, bandwidth, and efficiency," J. Res. Nat. Bur. Stand, vol. 64, no. 1, pp. 1–12, Jan.-Feb. 1960.

[10] S. Lim and H. Ling, "Design of electrically small Yagi antenna," Electron. Lett., vol. 43, no. 5, pp. 3-4, Mar. 2007.

[11] M. -C. Tang, N. Zhu and R. W. Ziolkowski, "Augmenting a modified Egyptian axe dipole antenna with non-Foster elements to enlarge its directivity bandwidth," IEEE Antennas Wireless Propag. Lett., vol. 12, pp. 421-424, 2013.

[12] T. Shi, M. C. Tang, Z. T. Wu, H. X. Xu, and R. W. Ziolkowski, "Improved signal-to-noise ratio, bandwidth-enhanced electrically small antenna augmented with internal non-Foster elements," IEEE Trans. Antennas Propag., vol. 67, no. 4, pp. 2763–2768, Apr. 2019.

[13] Y. -H. Yu, Z. -Y. Zong, W. Wu, and D. -G. Fang, "Dielectric slab superstrate electrically small antennas with high gain and wide band," IEEE Antennas Wireless Propag. Lett., vol. 19, no. 9, pp. 1476–1480, Sept. 2020.

[14] P. Jin, and R. W. Ziolkowski, "High-directivity, electrically small, low-profile near-field resonant parasitic antennas," IEEE Antennas Wireless Propag. Lett., vol. 11, pp. 305–309, 2012.

[15] M. -C. Tang, B. Zhou, Y. Duan, X. Chen, R.W. Ziolkowski, "Pattern-reconfigurable, flexible, wideband, directive, electrically small near-field resonant parasitic antenna," IEEE Trans. Antennas Propag., vol. 66, no. 5, pp. 2271-2280, May 2018.

[16] P. Jin and R. W. Ziolkowski, "Metamaterial-inspired, electrically small, Huygens sources," IEEE Antennas Wireless Propag. Lett., vol. 9, pp. 501-505, May 2010.

[17] R. W. Ziolkowski, "Low profile, broadside radiating, electrically small Huygens source antennas," IEEE Access, vol. 3, pp. 2644-2651, Dec. 2015.

[18] W. Lin and R. W. Ziolkowski, "Electrically-small, low-profile, Huygens circularly polarized antenna," IEEE Trans. Antennas Propag., vol. 66, no. 2, pp. 636-643, Feb. 2018.

[19] K. V. Caekenberghe, N. Behdad, K. M. Brakora, and K. Sarabandi, "A 2.45-GHz electrically small slot antenna," IEEE Antennas Wireless Propag. Lett., vol. 7, pp. 346–348, 2008.

[20] L. Salman, S. Salman, S. Jahangirian, M. Abraham, F. German, C. Blair, and P. Krenz, "Energy efficient IoT-based smart home," IEEE 3rd World Forum on Internet of Things (WF-IoT), pp. 526–529, 2016.

[21] C. S. Abella, S. Bonina, A. Cucuccio, S. D. Angelo, G. Giustolisi, A. D. Grasso, A. Imbruglia, G. S. Mauro, G. A. M. Nastasi, G. Palumbo, S. Pennisi, G. Sorbello, and A. Scuderi "Autonomous energy-efficient wireless sensor network platform for home/office automation," IEEE Sens. J., vol. 19, no. 9, pp. 3501–3512, May. 2019.

[22] A. Dierck, H. Rogier, and F. Declercq, "A wearable active antenna for global positioning system and satellite phone," IEEE Trans. Antennas Propag., vol. 61, no. 2, pp. 532–538, Feb. 2010.

[23] K. Cho and S. Hong, "Design of a VHF/UHF/L-band low-power active antenna for mobile handsets", IEEE Antennas Wireless Propag. Lett., vol. 11, pp. 45–48, 2012.

[24] W. T. Khan, A. L. Vera López, A. Ç. Ulusoy, and J. Papapolymerou, "Packaging a W-band integrated module with an optimized flip-chip interconnect on an organic substrate," IEEE Trans. Microw. Theory Techn., vol. 62, no. 1, pp. 64–72, Jan. 2014.

[25] N. Hasegawa, and N. Shinohara, "C-band active-antenna design for effective integration with a GaN amplifier," IEEE Trans. Microw. Theory Techn., vol. 65, no. 12, pp. 4976–4983, Dec. 2017.

[26] A. Erentok, and R. W. Ziolkowski, "Metamaterial-inspired efficient electrically small antennas," IEEE Trans. Antennas Propag., vol. 56, no. 3, pp. 691–707, Mar. 2008.

[27] A. J. Simmons and D. G. Bodnar, "Gain of active antenna systems: Antenna standards committee requests input," IEEE Antennas Propag. Soc. Newslett., vol. 31, no. 5, p. 62, Oct. 1989.

[28] D. Segovia-Vargas, D. Castro-Galán, L. E. García-Muñoz, and G. Posadas, "Broadband active receiving patch with resistive equalization," IEEE Trans. Microw. Theory Techn., vol. 56, no. 1, pp. 56–64, Jan. 2008.

[29] T. Macnamara, Introduction to Antenna Placement and Installation. Chichester, UK: John Wiley and Sons, 2010.

[30] A. D. Yaghjian and S. R. Best, "Impedance, bandwidth, and Q of antennas," IEEE Trans. Antennas Propag., vol. 53, no. 4, pp. 1298-1324, 2003.

[31] R. W. Ziolkowski, M. -C. Tang, and N. Zhu, "An efficient, broad bandwidth, high directivity, electrically small antenna," Microw. Opt. Technol. Lett., vol. 55, no. 6, pp. 1430–1434, Jun. 2013.

[32] N. Hasegawa, and N. Shinohara, "C-band active-antenna design for effective integration with a GaN amplifier," IEEE Trans. Microw. Theory Techn., vol. 65, no. 12, pp. 4976–4983, Dec. 2017.

[33] M. Gustafsson, C. Sohl, and G. Kristensson, "Physical limitations on antennas of arbitrary shape," Proc. R. Soc. A, vol. 463, pp. 2589–2607, 2007.

[34] M. Gustafsson, C. Sohl, and G. Kristensson, "Illustrations of new physical bounds on linearly polarized antennas," IEEE Trans. Antennas Propag., vol. 57, no. 5, pp. 1319-1327, 2009.

[35] R. W. Ziolkowski, "The directivity of a compact antenna: An unforgettable figure of merit," EPJ Appl. Metamat., vol. 4, 7, 2017.

[36] C. A. Balanis, Antenna Theory Analysis and Design, 3rd Edition, Hoboken: John Wiley & Sons, 2005.